SPE 143420

An Analytical Method for Predicting the Performance of Gravitationally-Unstable Flow in Porous Media

R. Farajzadeh, SPE and Shell Global Solutions International B.V., B. Meulenbroek, Delft University of Technology, J. Bruining, SPE and Delft University of Technology, The Netherlands

This paper was prepared for presentation at the SPE EUROPEC/EAGE Annual Conference and Exhibition held in Vienna, Austria, 23–26 May 2011.

Abstract

In this paper we follow a similar procedure as proposed by Koval (1963) to analytically model the performance of gravitationally unstable flow in porous media. The Koval model is analogous to the Buckley-Leverett method and multiplies the heterogeneity index of the system as an input (*H*-factor) with the fluid-flow (here gravity) induced instability factor, *E* to obtain the Koval factor $K_G = HE$. This paper only considers the gravity induced instability factor *E* ($H=1$). The Koval factor is implemented in a modified fractional flow function that includes a dilution effect when the CO_2 moves away from the interface to describe countercurrent gravity flow. The pseudo two-phase flow problem provides the average concentration of CO_2 in the brine as a function of distance. The K_G-factor can be used in commercial simulators to account for the density-driven natural convection, which cannot be currently captured because the grid cells are typically orders of magnitude larger than the wavelength of the initial fingers. Such natural convection effects occur in storage of greenhouse gases in aquifers and EOR processes using carbon dioxide or other solvents.

A comparison of the analytical model with the horizontally-averaged concentrations obtained from 2-D numerical simulations provides a correlation for calculation of the K_G-factor for different Rayleigh numbers. The model shows a rarefaction followed by shock-like behavior because the CO_2 concentration decreases away from the gaseous CO_2-liquid interface. The agreement between the analytical model and full numerical simulation is practically acceptable. We leave the introduction of the heterogeneity factor for future work.

Introduction

When a denser fluid is placed on top of a lighter one in the gravity field, it can lead to Rayleigh-Taylor instabilities (Taylor, 1950). This phenomenon is of importance for many fields of science and engineering (e.g. see Sharp, 1984); however, we confine our interest to CO_2-brine and CO_2-oil systems, relevant for CO_2 sequestration and enhanced oil recovery processes. The instabilities initiated by local density increase of brine (or oil), caused by dissolution of CO_2, increases the mass-transfer rate of CO_2 in brine (or oil) (Ennis-King and Paterson, 2000; Farajzadeh et al, 2007, 2009; Yang and Gu, 2006; Pau et al., 2010; Hassanzadeh et al., 2007; Neufeld et al., 2010; Riaz et al., 2006; Riaz and Tchelepi, 2006). The increase of the mass-transfer rate is equivalent to the dissolution of a larger amount of CO_2 in a shorter period of time and faster propagation of CO_2 in porous media (aquifers and hydrocarbon reservoirs). The large volume of dissolved CO_2 remains permanently in the liquid (at least as long as the pressure remains unchanged) and poses no threat of leakage, which is favorable for geological storage of CO_2.

Moreover, one of the challenges in the application of chemically-enhanced oil recovery methods for the naturally fractured reservoirs using solvents is the slow mass transfer between the solvent in the fracture and the crude oil in the matrix. By injecting a solvent that is miscible with oil and increases the density of oil (for instance CO_2), natural convection phenomenon could enhance the transfer rates, increase the mixing between the solvent and the oil, and accelerate the oil production. Naturally, the time required for the initiation of the convection and in case of injection of costly solvents the recycling of the solvent play a crucial role in the (economic) success of the proposed method of oil production.

The efficiency of mixing in density-driven natural convection is governed by the Rayleigh number, which includes the reservoir permeability and the density difference. Stability analysis of the saturated porous layers under density-driven natural convection effects indicates that the time required for the initiation of natural convection is proportional to ~ Ra^{-2} and the critical wavelength is proportional to ~ Ra^{-1} (Meulenbroek et al, 2011; Riaz et al., 2006). The critical wavelength, λ_c, in an indication of the grid size required to capture the initiation of the initial fingers. Let us define Rayleigh number by:

$$Ra = \frac{k\Delta\rho g H}{\varphi \mu_w D} \quad . \tag{1}$$

For the typical values of (k = 1 Darcy, $\Delta\rho$ = 10 kg/m^3, g = 10 m/s^2, H = 50 m, μ_w = 1 cP, $D = 2\times10^{-9}$ m^2/s, and φ = 0.2) we obtain: $Ra = 1.25\times10^4$, which using the analysis of Meulenbroek et al. (2011) provides: λ_c = 110H / Ra ~ 0.009H = 50 cm. This implies that accurate estimation of the amount of dissolved CO_2 in brine under these conditions requires grid sizes much smaller than 50 cm. For highly permeable and heterogeneous porous media the required grid size may be too small to resolve even with massively parallel architectures (Lu and Lichtner, 2007; Pau et al., 2010). This necessitates the development of simpler models that could approximately quantify the amount of dissolved CO_2 after injection period taking into account the instabilities.

In miscible displacement the viscosity difference between the solvent and the oil leads to development of fingers that adversely affects the oil recovery. Because of the fingering behavior the evolution of concentration of the solvent cannot be predicted by fractional-flow-based miscible displacement models, originally described by Peaceman and Rachford (1962). Koval (1963) developed a simple model to account for the instabilities (fingering behavior) observed in the miscible displacements. In his model the fractional-flow function in the Buckley-Leverett equation is replaced by:

$$f_{koval}\left(c\right) = \frac{1}{1 + \dfrac{1-c}{c}\dfrac{1}{K_G}} \quad , \tag{2}$$

where the Koval factor $K_G = H_k E$. Here E is the “effective” viscosity ratio and is defined as the ratio between the oil viscosity and the viscosity of mixture of oil and solvent in which the volume fraction of the solvent is c_e. It turns out from experimental results that c_e=0.22. E is chosen such that the results of the model fit the experimental data. For heterogeneous reservoirs E is multiplied by the Koval heterogeneity index, H_k, which is related to the Dykstra-Parson’s coefficient by

$$\log H_k = \frac{V_{DP}}{(1 - V_{DP})^{0.2}} \quad . \tag{3}$$

The degree of the heterogeneity of the permeability field determines the character of the density-driven natural convection flow in porous media. Similar to the instabilities induced by the viscosity difference between the fluids (Waggonner et al; 1991), instabilities induced by a density difference can lead to *fingering, channeling*, and *dispersive* regimes depending on the degree of the permeability variance (Dykstra-Parsons coefficient) and the correlation length of the porous medium (Farajzadeh et al, 2011; Ranganathan et al; 2011). The dispersive regime (characteristic of flow in media with a high degree of heterogeneity) can be analytically modeled by choosing an effective dispersion coefficient in a diffusion-based model. In the channeling regime, which occurs for medium degree of heterogeneity, there is no correlation with the measures of heterogeneity and the transfer rate of CO_2 in water and therefore the method proposed by Koval cannot be applied without modification. Here, we confine our interest to find an analytical model for low degree of heterogeneity, which leads to fingering regime. It could be validated that for a low degree of heterogeneity the effect of heterogeneity on the transfer rate is relatively small.

The objective of this paper is to develop an analytical model that predicts the performance of gravitationally unstable flow in porous media. Our special focus will be on the inclusion of the effect of fingering on the transfer rate of CO_2 in brine. We use an analogous procedure as proposed by Koval (1963). The proposed model is similar to the Buckley-Leverett method for gravity dominated flow. The flow function uses a “gravity fingering index” as an input (K_G-factor). The solution provides the average concentration of CO_2 in the brine as a function of distance and eventually the total mass of dissolved CO_2. The structure of the paper is as follows. First we describe the physical model and provide the ensuing equations. Next we use method of matched asymptotic expansions to obtain an approximate analytical solution for most of the described equations. Afterwards, we introduce empirical parameters into the model to take into account the fingering behavior and compare the results of the proposed model to the numerical simulations. Finally we draw the main conclusions of this study.

2. Physical Model

Figure 1 schematically shows the purpose of the model, i.e., to capture the averaged behavior of the process in the direction of the flow. If there is no instability, there will be a short transition zone (here the ensuing error function is represented as a shock) between the CO_2 containing brine and the initial brine that contains no CO_2. This occurs when the flow regime is diffusive (e.g. at initial stages of the process) or dispersive (for highly heterogeneous media). This behavior can be accurately modeled through diffusion-based models, albeit with an effective diffusion coefficient. When instabilities occur, the concentration front moves faster and there is a gradual change from high (horizontally averaged) concentration of CO_2 at the top to the initial concentration.

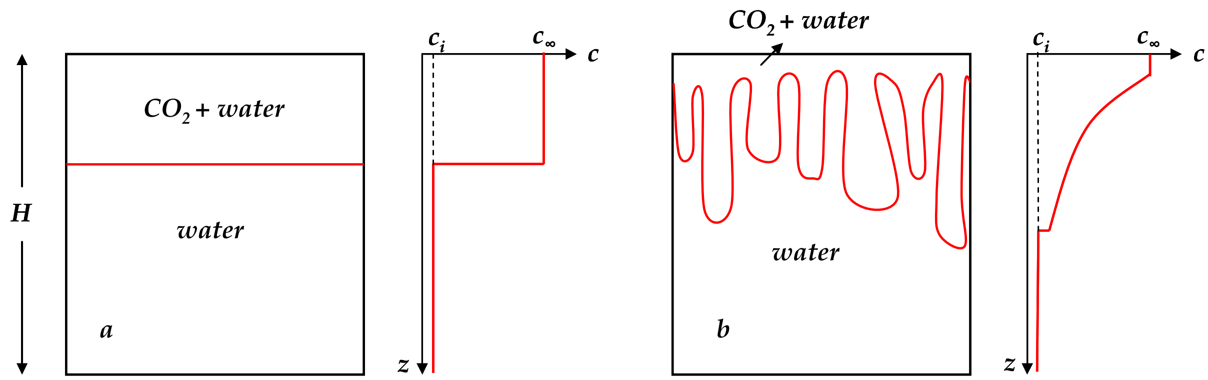

Figure 1: schematic of (a) stable and (b) unstable displacement and transverse average of the corresponding concentration profiles.

2.1. Formulation

We consider a one-dimensional porous medium of length H that is initially saturated with water. The vertical coordinate, z, is taken positive in the downward direction. The constant porosity of the porous medium is φ and its permeability is k. Initially there is no CO_2 dissolved in water ($c_i = 0$). We assume a no flow boundary at the bottom of the porous medium. CO_2 is continuously supplied from the top, i.e., the CO_2 concentration at the top is kept constant and therefore the water at the interface is fully saturated with CO_2. The water and water saturated with CO_2 (referred to as "*mixture*" and represented by m) are considered as two separate phases; (1) pure water with density ρ_w and viscosity μ_w and (2) a mixture phase with density ρ_m and viscosity μ_m. We disregard the presence of a capillary transition zone between water and mixture phases and assume that the relative permeability of the mixture is proportional to its saturation denoted by S_m. In the same way is the relative permeability of the water phase proportional to its saturation $S_w = 1 - S_m$.

2.2. Governing Equations

The motion of fluids in a porous medium can be described by Darcy's law. The Darcy equation for the mixture can be written as

$$u_m = -\lambda_m \left(\frac{\partial p_m}{\partial z} - \rho_m g \right) \quad . \tag{4}$$

The Darcy equation for water reads

$$u_w = -\lambda_w \left(\frac{\partial p_w}{\partial z} - \rho_w g \right) \quad . \tag{5}$$

where u is the Darcy velocity, p_α, $(\alpha = m, w)$ is the pressure of phase α, ρ_α is the density of phase α, and g is the acceleration due to gravity, and $\lambda_\alpha = kk_{r\alpha} / \mu_\alpha$ $(\alpha = m, w)$ is the mobility, which is the ratio between the phase permeability $kk_{r\alpha}$ and the viscosity μ_α. Subscripts m and w denote the CO_2+water mixture and the initial water, respectively. Both viscosity and density are assumed to be functions of the CO_2 concentration.

The saturated density difference between an aqueous solution of CO_2 and pure water is given by $c_\rho P_g$, where the value of the c_ρ = 0.261 kg/ m^3 / bar for pure water (see Gmelin p 72). c_ρ will be less for formation brines, because the solubility of CO_2 in water decreases with increasing salinity. Therefore, the density of the mixture can be assumed to increase according to the following relationship:

$$\Delta\rho = \rho_m - \rho_w = c_\rho P_g S_m^n , \tag{6}$$

where S_m^n represents a dilution effect as the gravity fingers move away from the interface.

The saturation exponent n can have values between 0 and 1. We assume ideal mixing and use Boussinesq approximation, i.e., we only consider the density variations in Eqs. (4) and (5). With this assumption and because there is no source or sink in our model, the volume conservation is equivalent to mass conservation and hence

$$u_m + u_w = 0 \quad , \tag{7}$$

which implies a countercurrent flow. We can derive an expression for the Darcy velocity of the mixture, i.e.,

$$u_m + u_w = 0 = u_m - \frac{\lambda_w}{\lambda_m}\lambda_m\left(\frac{\partial p}{\partial z} - \rho_m g\right) - \lambda_w\left(\rho_m - \rho_w\right)g \, . \tag{8}$$

Hence it follows that

$$u_m = \frac{\lambda_w \lambda_m}{\lambda_w + \lambda_m}(\rho_m - \rho_w)g \quad . \tag{9}$$

The conservation law for the mixture including diffusion reads:

$$\varphi\frac{\partial S_m}{\partial t} + \frac{\partial u_m}{\partial z} = \varphi D\frac{\partial^2 S_m}{\partial z^2} \quad . \tag{10}$$

Replacing Eq. (9) in Eq. (10) leads to

$$\varphi\frac{\partial S_m}{\partial t} + \frac{\partial}{\partial z}\left(\frac{\lambda_w \lambda_m}{\lambda_w + \lambda_m}(\rho_m - \rho_w)g\right) = \varphi D\frac{\partial^2 S_m}{\partial z^2} \quad . \tag{11}$$

2.3. Dimensionless form of the equations

We scale the velocity with a characteristic velocity $u_c = kc_\rho P_g g / \mu_w$, length with H, and t with $\varphi H / u_c$. Therefore, Eq. (11) leads to:

$$\frac{\partial S_m}{\partial \tau} + \frac{\partial}{\partial \xi}\left(\frac{S_m^n k_{rw}}{\Lambda^{-1} + 1}\right) = \varepsilon\frac{\partial^2 S_m}{\partial \xi^2} \tag{12}$$

where $\tau = (u_c / \varphi H)t$, $\xi = z / H$, $\Lambda = \lambda_m / \lambda_w$, $\varepsilon = 1/Pe$, and $Pe = u_c H / D = Ra$. We define the "fractional flow function" as

$$f\left(S_m\right) = \frac{S_m^n k_{rw}}{\Lambda^{-1} + 1} \quad . \tag{13}$$

Therefore, Eq. (12) can be written as

$$\frac{\partial S_m}{\partial \tau} + \frac{\partial f(S_m)}{\partial S_m}\frac{\partial S_m}{\partial \xi} = \varepsilon\frac{\partial^2 S_m}{\partial \xi^2} \quad . \tag{14}$$

The Peclet number, *Pe*, is defined as the ratio between the convective and diffusive fluxes. For typical values mentioned earlier we will obtain $u_c = 2\times10^{-7}$ m/s. Using $D = 2\times10^{-9}$ m^2/s we obtain: $Pe = 5000$. Zimmerman and Homsy (1992) noted that for $Pe >> 1$

it is reasonable to model diffusion as constant and isotropic because at large Peclet numbers all averaged quantities are independent of any anisotropy (see also Booth, 2008). Hence taking D as constant is justified. We notice that for very large Peclet numbers ($Pe \to \infty$ or $\varepsilon \to 0$) Eq. (14) converts to the classical Buckley-Leverett equation, albeit with a different fractional-flow function.

At the displacement problems the initiation of the flow is forced by injection. In our case, the flow rate cannot be forced. Therefore a crucial parameter of the model is to define the top boundary condition. If we assume that the saturation of the mixture is one, it is not immediately clear how unstable convective motion would initiate. Here we will investigate the approximate analytical solution of Eq. (14) with the method of matched asymptotic expansions and compare it with the numerical solution. The method is briefly explained in Appendix A.

2.4. Approximate solutions

The approximate solution consists of an inner solution in the domain $R_1 = [0, \varepsilon)$, where diffusion dominates and an outer solution in $R_2 = (\varepsilon, 1]$ that is convection dominated. It turns out that the outer solution consists of a rarefaction solution combined with a shock and that the inner solution concerns the stationary diffusion equation.

2.4.1. Rarefaction (or outer) and shock solutions

In the absence of diffusion the solution consists of rarefactions, constant states and shocks. Firstly, we derive the rarefaction solution and the constant state. We can use a coordinate transformation $\eta = \xi / \tau$ and obtain from Eq. (14)

$$\left(-\eta + \frac{df(S_m)}{dS_m}\right)\frac{\partial S_m}{\partial \eta} = 0 \qquad . \tag{15}$$

The solution of Eq. (15) is either a constant state $dS_w / d\eta = 0$ or

$$\eta = \frac{df(S_m)}{dS_m} \qquad . \tag{16}$$

This equation can be solved to obtain $S_m = S_m(\eta)$ on condition that the second derivative of the fractional-flow function does not change the sign (Landau and Lifshitz, 1959; Silin et al., 2009), i.e., in the absence of shocks. Replacing the parameters in Eq. (13) we obtain

$$\eta = \frac{d}{dS_m}\left(\frac{(1 - S_m)S_m^n}{\dfrac{(1 - S_m)}{S_m}\dfrac{1}{K_G} + 1}\right) \quad , \tag{17}$$

where, we have replaced μ_w / μ_m with K_G similar to Koval (1963). The term in brackets is plotted in Figure 2. At downstream of the diffusive layer, the solution of Eq. (17) for different values of K_G starts at the saturation corresponding to the highest phase velocity (maximum of the fraction-flow function) with a rarefaction solution. We refer to K_G as the "gravity fingering index" and it can be used as fitting parameter to obtain agreement between the numerical and analytical results. The solution will include a shock for $n > 0$. The general rarefaction solution of Eq. (17) is

$$\eta = \left(-\frac{S_m^n}{\frac{(1-S_m)}{S_m}\frac{1}{K_G}+1} + \frac{n(1-S_m)S_m^n}{S_m\left(\frac{(1-S_m)}{S_m}\frac{1}{K_G}+1\right)} + \frac{1}{K_G S_m}\frac{(1-S_m)S_m^n\left(1+\frac{1-S_m}{S_m}\right)}{\left(\frac{(1-S_m)}{S_m}\frac{1}{K_G}+1\right)^2} \right). \quad (18)$$

For $K_G = 1$, i.e., $\mu_m = \mu_w$ and $n = 0$ the solution is simplified to:

$$\eta = (1 - 2S_m) \quad , \quad (19)$$

or

$$S_m = \frac{1}{2}(1-\eta) = \frac{1}{2}\left(1 - \frac{\xi}{\tau}\right) = \frac{1}{2}\left(1 - \frac{\varphi\mu_w}{k(\rho_m - \rho_w)g}\frac{z}{t}\right). \quad (20)$$

The rarefaction solution will be followed by a shock if n has a non-zero value. The shock occurs when the following condition is satisfied:

$$\frac{f(S_{m,shock})}{S_{m,shcok}} = \frac{df(S_m)}{dS_m} \quad , \quad (21)$$

where we have assumed that initially there is no CO_2 dissolved in the brine. Using Eq. (13) the shock saturation equals:

$$S_{m,shock} = \frac{1}{2}\frac{K_G(n-1) - 2n + \sqrt{K_G^{\,2}(n-1)^2 + 4K_G n}}{n(K_G - 1)} \quad . \quad (22)$$

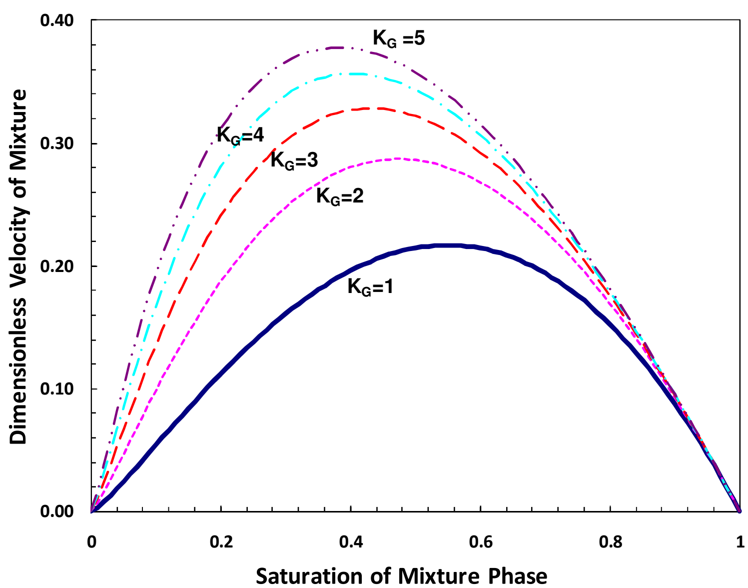

Figure 2: Plot of dimensionless phase velocity, i.e., term in brackets in RHS of Eq. (17) versus saturation. We use *n*=0.22. Just downstream of the diffusion layer all solutions start at the saturation corresponding to the highest phase velocity with a rarefaction possibly followed by a shock.

2.4.2. Diffusion equation (or inner) solution

In R_1 we rescale the z-coordinate: $X = \dfrac{\xi}{\varepsilon}$ in Eq. (12). This leads to

$$\varepsilon \frac{\partial S_m^{in}}{\partial \tau} + \frac{\partial f\left(S_m^{in}\right)}{\partial X} = \frac{\partial^2 S_m^{in}}{\partial X^2} \quad . \tag{23}$$

The term $\varepsilon \partial S_m^{in} / \partial \tau$ is small with respect to the other terms and can be omitted. There Eq. (25) becomes

$$\frac{\partial f\left(S_m^{in}\right)}{\partial X} = \frac{\partial^2 S_m^{in}}{\partial X^2} \quad . \tag{24}$$

Integration of Eq. (24) gives

$$\frac{\partial S_m^{in}}{\partial X} = f(S_m) + \kappa \quad , \tag{25}$$

where, κ is a constant. The matching condition reads (Verhulst, 2000; van Dyke, 1975):

$$\lim_{X \to \infty} S_m^{in}\left(X\right) = \lim_{\xi \to 0} S_m^{out}\left(\xi\right) = S_m^0 \quad .$$

From Eq. (15) we have:

$$\eta = 0 \to S_m^0 = \frac{1}{2} \frac{-2\left(n+1\right) + nK_G + \sqrt{4K_G\left(n+1\right) + n^2 K_G^2}}{\left(n+1\right)\left(K_G - 1\right)} . \tag{26}$$

S_m^0 is the saturation that separates the diffusive and rarefaction regimes. Notice that this is the saturation where the fractional-flow function attains its maximum. The second boundary for Eq. (24) reads: $S_m^0\left(0\right) = 1$. Expanding Eq. (24) gives

$$\frac{dS_m^{in}}{dX} = f\left(S_m^{in}\right) + \kappa = \frac{(S_m^{in})^{n+1} K_G - (S_m^{in})^{n+2} K_G + \kappa K_G S_m^{in} + \kappa - \kappa S_m^{in}}{K_G S_m^{in} + 1 - S_m^{in}} . \tag{27}$$

We only get bounded solution when

$$\lim_{X \to \infty} \frac{dS_m^{in}}{dX} = \lim_{X \to \infty} \left(f(S_m^{in}) + \kappa \right) = 0 \quad . \tag{28}$$

This means that

$$\kappa = -f(S_m^0) \quad . \tag{29}$$

Replacing κ in Eq. (25) and using the definition of the fractional-flow function in Eq. (13) we obtain

$$\int_1^\infty dX = \int_1^{S_m^0} \frac{dS_m^{in}}{f(S_m^{in}) - f(S_m^0)} \quad . \tag{30}$$

Explicit integration of Eq. (30) is not trivial and should be solved numerically for different values of n and K_G to obtain the saturation profile. Nevertheless, for $n = 0$ and $n = 1$ it is possible to find an analytical solution. For $n = 1$ and $K_G = 1$, Eq. (26) gives: $S_m^0 = 1 / 2$ and the inner solution is simplified to

$$S_m^{in}(X) = \frac{X + 4}{2X + 4} \quad . \tag{31}$$

Figure 3 plots the inner solution (Eq. 31) and outer solution (Eq. 19) of this case and compares it to the numerical solution. For n=1 and K_G = 1, the asymptotic value of the saturation is 2/3.

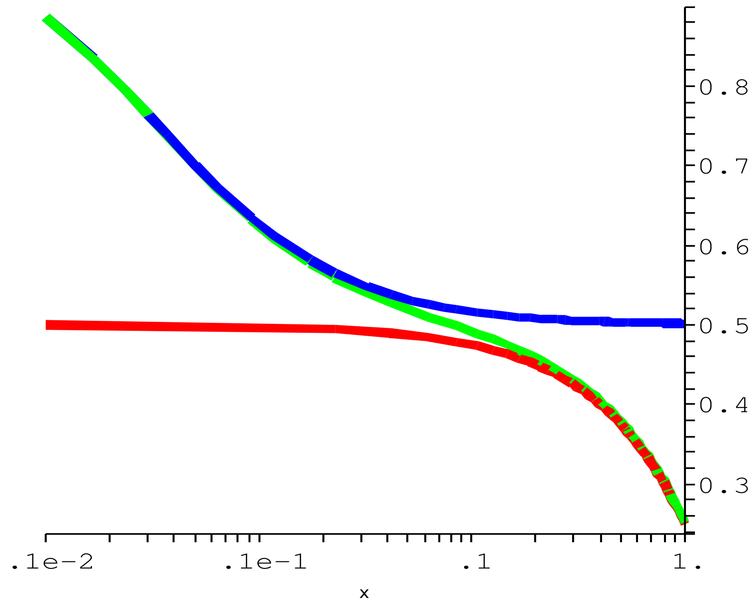

Figure 3: Inner solution (Eq. 31) and outer solution (19) and numerical solution of Eq. (12) for Pe = 5000.

Results and Discussion

In this section we present the results of the 1-D analytical model and compare them to the results of the numerical simulations, which were performed on a 2-D porous medium with an aspect ratio of 1. A no-flow boundary condition was used at the sides and at the bottom of the medium. The concentration of CO_2 at the top of the medium was assumed to be 1. To observe the fingering behavior the interface was initially perturbed. A fully implicit finite volume approach (Guçeri and Farouk, 1985) was used to solve the equations. The details of the numerical simulations can be found in Farajzadeh et al. (2007, 2011).

To compare the results, the concentration values of the 2D numerical simulations were averaged in the horizontal direction. An example is shown in Figure 4. The simulation of diffusion part of the problem requires grid cells that are in the order of *1/Ra* in the vertical direction. Our numerical simulation consists of 81×81 grid cells and therefore we are not able to accurately model the diffusive regime, which is dominant before onset of the natural convection. However, this does not affect the estimated transfer rate (Farajzadeh et al., 2009).

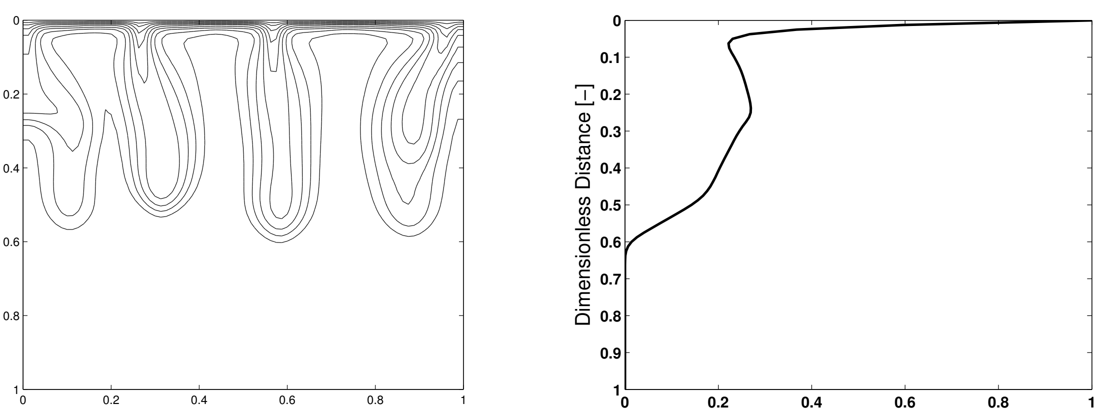

Figure 4: The concentration profile of CO_2 for *Ra* = 2000 at τ = 6. The right plot is obtained by averaging the concentration value of left plot in the horizontal direction.

Figure 5 through Figure 8 demonstrate the concentration profiles of CO_2 at different times for different Rayleigh numbers. The solid and dashed lines are the results of the analytical model and the numerical simulations, respectively. To consider the effect of fingering the dimensionless time should be scaled with the time-scaling factor, α_τ, in Eq. (18). This assures that the concentration front moves faster when fingering occurs. The agreement between the two models is acceptable, especially for lower Rayleigh numbers. We note from Figure 3 that the asymptotic saturation value S_m near $z=0$ of the model is between 0.5 (for n = 0) and 2/3 (n = 1). However, the horizontally-averaged concentrations obtained from 2-D numerical simulations converge at a smaller value than this saturation value. The saturation value decreases further with increasing Rayleigh number. For higher Rayleigh numbers the value decreases to even smaller values as time progresses. Therefore, to obtain a reasonable match between the analytical and numerical models, the K_G-factor was modified such that the asymptotic values of the saturation values S_m near the interface of the two models matched. We ignored time dependency of this value, i.e., we kept K_G –factor independent of time. It is interesting to mention that the best fit was obtained for n = 0.22 (Eq. 6) for all simulations. The other fitting parameters, i.e., K_G and α_τ, are listed in Table 1. The K_G-factor increases with increasing Rayleigh number. Moreover, with increasing Rayleigh number the effect of convective mixing (gravity induced instability) becomes more pronounced and therefore the time required for CO_2 front to reach the bottom of the medium decreases (Riaz et al., 2006; Farajzadeh et al., 2007). On the other hand the density of the mixture increases with increasing Rayleigh number (Eq. 1). This means that the time-scaling factor (α_τ) includes both of these effects.

Note that our model is only valid until CO_2 reaches the bottom of the medium. After this time CO_2 saturated solution will start to fill up the layer from the bottom. This filling up has been treated in a pioneering paper of Siddiqui and Lake (1997) and later by Bedrikovetsky et al. (2001), who addressed an analogous problem concerning the secondary migration of oil. Oil was moving through countercurrent gravity drainage from the source rock to the future reservoir initially filled with water. The problem is almost the same as the problem considered here except that the saturation exponents of the relative permeabilities are not one for the true two-phase (oil and water) conditions and the trivial fact that the gravity is pointing in the opposite direction. Another main difference is that in the migration problem the upstream boundary condition (in the source rock) is that the oil saturation is a given low value and is not governed by a diffusion process like here. Downstream there is a seal, which may be partially leaking, which is one of the complicating factors in the paper by Siddiqui and Lake (1997). In our case we assumed a no-flow boundary at the bottom.

In analogy of the Siddiqui-Lake paper we expect that a reflected wave will occur once the CO_2 saturated solution hits the bottom of the reservoir. Indeed, the saturation of the carbon dioxide containing aqueous phase near the bottom will increase until it is in the right side of Figure 2. Here the wave velocity (see Eq. (17)) will be negative (reflected wave). Consequently the reservoir will stably fill up from the bottom with the saturated solution. This aspect will be left for future work.

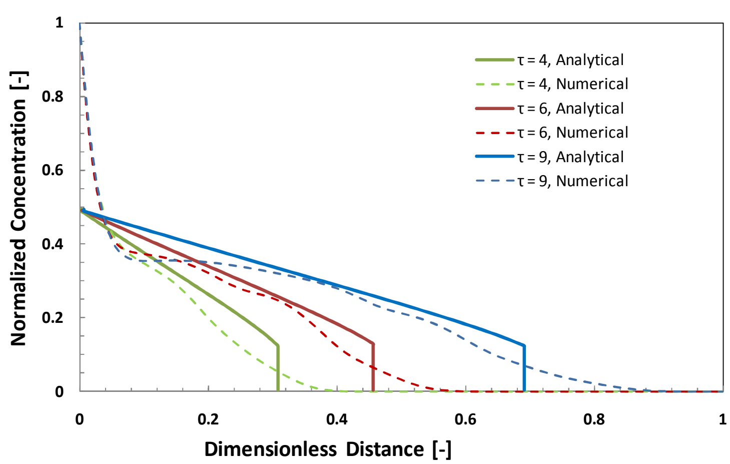

Figure 5: Comparison between the analytical (solid lines, n=0.22. K_G=1.66, α_τ =0.8) and numerical (dashed lines) models at different times for Ra = 1000.

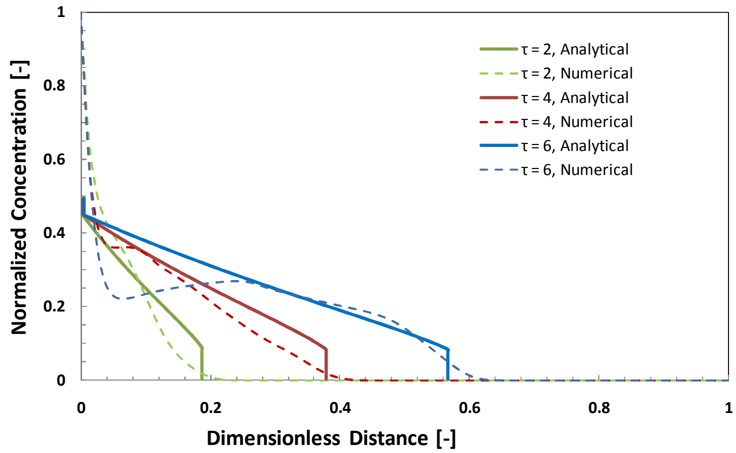

Figure 6: Comparison between the analytical (solid lines, n=0.22. K_G = 2.6, α_τ =0.45) and numerical (dashed lines) models at different times for Ra = 2000.

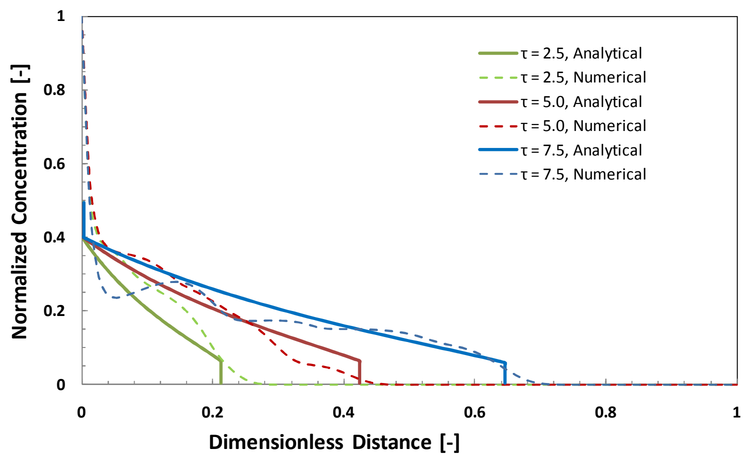

Figure 7: Comparison between the analytical (solid lines, n=0.22. K_G = 4.0, α_τ =0.37) and numerical (dashed lines) models at different times for Ra = 5000.

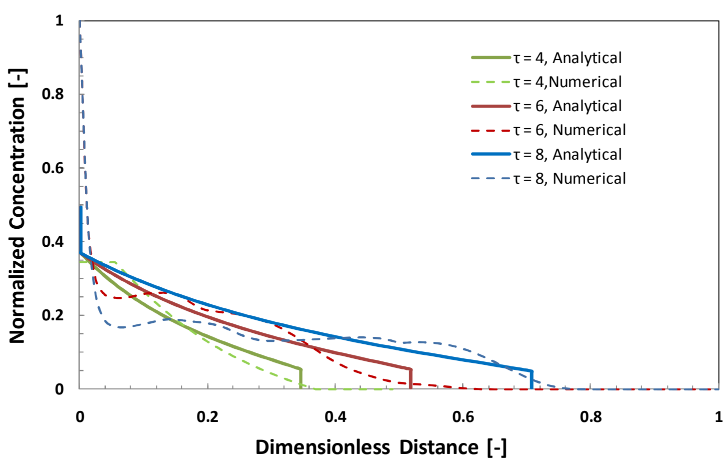

Figure 8: Concentration profiles obtained from the analytical (solid lines, n = 0.22. K_G = 5.6, α_τ = 0.25) and numerical (dashed lines) models at different times for Ra = 10000.

Table 1: The values of K_G and α_τ used as fitting parameters to obtain the match between the analytical and numerical models.

Rayleigh Number	α_τ	K_G
1000	0.80	1.66
2000	0.45	2.6
5000	0.37	4.0
10000	0.25	5.6

In Figure 9 we plot the parameters reported in Table 1 as a function of Rayleigh number. The fitting exercise provides the following relationships

$$K_G = 0.042 Ra^{0.532}, \quad \alpha_\tau = 6.85\ Ra^{-0.436} \quad . \tag{32}$$

These empirical relations can be used to "effectively" model the gravity-induced instabilities.

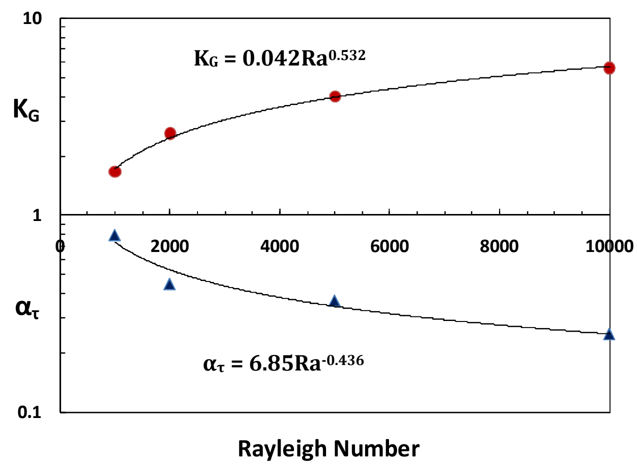

Figure 9: The fitting parameters as a function of Rayleigh number.

Figure 10 plots the mass of the dissolved CO_2 (normalized to the maximum mass that can be dissolved) for different Rayleigh numbers and compares it to the numerical model. For illustration purposes, the time has been divided to the corresponding Rayleigh number of each case. The analytical model is less accurate for the higher Rayleigh numbers. The disagreement is more pronounced at the initial stages and the analytical model under-predicts the dissolved mass. One possible reason for this is that the analytical model only consists of a convection part and there is no diffusion in the model. As mentioned earlier the transfer at the initial stages of the process is governed by diffusion. The numerical model, however, might over-predict the dissolved mass due to numerical dispersion.

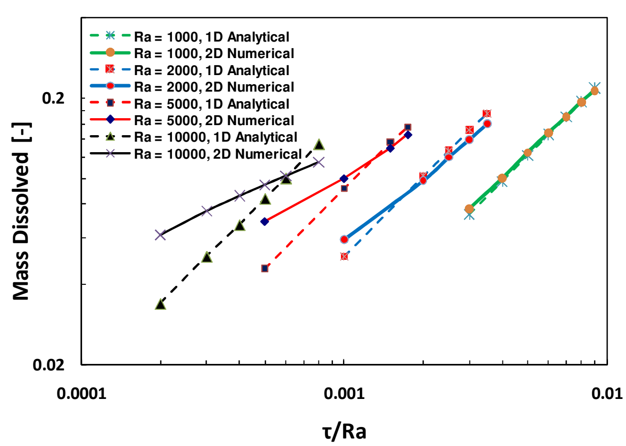

Figure 10: The mass of CO_2 dissolved in water obtained from the analytical (dashed lines) and numerical (solid lines) models at different times for different Rayleigh numbers.

Conclusions

- Following a similar procedure as proposed by Koval (1963) we developed an analytical model to predict the performance of gravitationally unstable flow in porous media,
- The method of matched asymptotic expansions was used to obtain an approximate analytical solution for the relevant equations describing the diffusive and convective regimes. The analytical solution is in good agreement with the numerical results.
- The developed model takes the "gravity fingering index" (or K_G-factor), a time-scaling factor α_τ, and a saturation exponent, n, as input parameters and provides the average concentration of CO_2 in the brine as a function of distance at different times.
- A comparison between the analytical model and the horizontally-averaged concentrations obtained from 2-D numerical simulations provides a correlation for calculation of the K_G-factor and the time-scaling factor α_τ for different Rayleigh numbers. The saturation exponent is $n = 0.22$ for all cases.
- The model shows a rarefaction followed by shock-like behavior because the concentration in the fingers decreases (n=0.22) away from the gaseous CO_2-liquid interface. The agreement between the Koval procedure and full numerical simulation is practically acceptable.
- The empirical relations between the K_G-factor and the Rayleigh number, and the time-scaling factor α_τ and the Rayleigh number can be used in commercial simulators to account for the density-driven natural convection, which cannot be currently captured because the grid cells are typically orders of magnitude larger than the wavelength of the initial fingers.

Acknowledgments

This work was made possible by support of the Dutch national research programme CATO 2 on CO_2 capture, transport and storage: Work Package 3.02: Reservoir behavior. The first author thanks Shell Global Solutions International B.V. for granting permission to publish this work.

Nomenclature

c	Dimensionless concentration [-]
D	Diffusion coefficient [m^2/s]
E	Effective viscosity ratio
f	Fractional-flow function
g	acceleration due to gravity [m/s^2]
H	Height of the porous medium [m]
H_k	Koval heterogeneity factor [-]
k	Permeability of the porous medium [m^2]
k_r	Relative permeability [-]
K	Koval factor
K_G	Gravity fingering index
p	Pressure [Pa]
Pe	Peclet number [-]
Ra	Rayleigh number [-]
S	Phase saturation [-]
t	Time [sec]
u_c	Dimensionless velocity [-]
u	Velocity [m/s]
V_{DP}	Dykstra-Parsons coefficient
X	Re-scaled z coordinate (ξ/ε)
z	Distance in z coordinate

Greek symbols

α_τ	Time-scaling factor
ε	$1/Pe$
φ	Porosity of the porous medium [-]

η Transformation coordinate
λ_c Wavelength [m]
λ Mobility (k_r/μ)
Λ Mobility ratio of phase [-]
μ Viscosity of the fluid [kg/m-sec]
ξ Dimensionless distance (z/H)
ρ Density of the fluid [kg/m^3]
τ Dimensionless time [-]

Subscripts

$_i$ Initial value of the quantity
$_m$ Mixture phase
$_s$ Pure solvent
$_w$ Water phase
$_z$ Quantity in z-direction

References

Bedrikovetsky, P.; De Deus, J.; Eurico Altoé, J.: *Secondary migration of oil: analytical model*. *SPE 69411*. In: 2001 SPE Latin American and Carribean petroleum engineering conference, Buenos Aires, Argentina, SPE (2001).

Booth, R. Miscible flow through porous media. PhD dissertation, University of Oxford (2008).

Ennis-King, J. and Paterson, L.; *Role of convective mixing in the long-term storage of carbon dioxide in deep saline aquifers*, SPE J 10 (3) (2005) 349.

Farajzadeh, R. Salimi, H, Zitha, P.L.J. and Bruining, J.. "*Numerical simulation of density-driven natural convection in porous media with application for CO_2 injection projects",* Int. J. Heat Mass Trans., Vol. 50, Issues 25-26 (2007b), Pages 5054-5064.

Farajzadeh, R. Barati, A., Delil, H.A.. Bruining, J. and Zitha, P.L.J., "*Enhanced mass transfer of CO_2 into water and surfactant solutions",* Petroleum science and technology, Vol. 25, Issue 12 (2007) pages 1493 – 1511.

Farajzadeh, R. Farshbaf Zinati, F., Zitha P.L.J., and Bruining, J., Density-driven Natural Convection in Dual Layered and Anisotropic Porous Media with Application for CO_2 Injection Projects, A40 ECMOR XI. 8 - 11 September 2008, 11th European Conference on the Mathematics of Oil Recovery. Bergen, Norway.

Farajzadeh, R., Bruining, J., and Zitha, P.L.J. , *Enhanced mass transfer of CO_2 into water: experiment and modeling,* Ind. Eng. Chem. Res. **48** (9) (2009) 4542-455.

Farajzadeh, R.; Ranganathan, P; Zitha P.L.J. and Bruining, J. *The Effect of Heterogeneity on the Character of Density-Driven Natural Convection of CO_2 Overlying a Brine Layer.* Advances in Water Resources, 34(3) (2011) 327-339.

Gmelin L., *Gmelin Handbuch der anorganischen Chemie*, 8. Auflage. Kohlenstoff, Teil C3, Verbindungen., pp 64-75 (1973).

Guçeri S. and Farouk B., *Numerical solutions in laminar and turbulent natural convection,* In: Natural convection, Fundamentals and applications, S. Kakac, W. Aung, R. Viskanta, Hemisphere publication, 615-655 (1985).

Hassanzadeh, H; M Pooladi-Darvish, D Keith. *Scaling behavior of convective mixing, with application to CO2 geological storage*. AIChE Journal 53 (5) (2007) 1121-1131.

Koval, E. J. *A Method for Predicting the Performance of Unstable Miscible Displacement in Heterogeneous Media.* SPE J. 3(2) (1963) 145-154.

Landau, L.D. and Lifshitz, E.M. Course of Theoretical Physics. Fluid Mechanics. Series in Advanced Physics, vol. 6. Addison-Wesley, Reading (1959).

Lu, C. and Lichtner, P.C. High resolution numerical investigation on the effect of convective instability on long term CO_2 storage in saline aquifers. *J. Physics: Conference Series* 78 (2007) 12042.

Meulenbroek, B.; R. Farajzadeh; J. Bruining, *Multiple scale analysis of the stability of a* diffusive *interface between aqueous and gaseous CO_2*, Submitted to J. Fluid Mechanics, 2011.

Neufeld, J.A., Hesse, M.A., Riaz, A., Hallworth, M.A., Tchelepi, H.A., Huppert, H.E., Convective dissolution of carbon dioxide in saline aquifers, Geophysical Research Letters 37 (22) (2010) art. no. L22404.

Pau, G.S.H., Bell, J.B., Pruess, K., Almgren, A.S., Lijewski, M.J., Zhang, K., *High-resolution simulation and characterization of density-driven flow in CO_2 storage in saline aquifers*, Advances in Water Resources 33 (4) (2010) 443-455.

Peaceman, D.W. and Rachford Jr., H.H. Numerical calculation of multi-dimensional miscible displacement. Society of Petroleum Engineers J., 2 (1962) 327–339.

Ranganathan, P.; Farajzadeh, R.; Bruining, J.;. Zitha, P.L.J. *Numerical Simulation of Natural Convection in Heterogeneous Porous media for CO_2 Geological Storage.* To be published in Transport in Porous Media (2010).

Riaz, A., Tchelepi, H.A., *Dynamics of vertical displacement in porous media associated with CO_2 sequestration*, Proceedings - SPE Annual Technical Conference and Exhibition 6 (2006) 4298-4309.

Riaz A., Hesse M., Tchelepi A. and Orr F.M., *Onset of convection in a gravitationally unstable diffusive boundary layer in porous medium,* J. Fluid Mech., 548 (2006) 87-111.

Siddiqui, F.I. and Lake, L.W. *A comprehensive dynamic theory of hydrocarbon migration and trapping*. *SPE 38682.* In: 1997 72th annual technical conference and exhibition, San Antonio, TX, SPE (1997).

Silin, D.; Patzek, T. and Benson, S.M. A Model of Buoyancy-Driven Two-Phase Countercurrent Fluid Flow. Transp. Porous Med 76 (2009) 449–469.

Sharp, D.H. *An overview of Rayleigh-Taylor instability*, Physica 12D (1984) 3-18.

Taylor, G.I., *The instability of liquid surfaces when accelerated in a direction perpendicular to their planes*. Proc. R. Soc. Lond. Ser. A 201 (1950) 192–96.

Van Dyke, M. *Perturbation methods in fluid mechanics.* The Parabolic Press (1975), Stanford California

Verhulst, F. *Methods and applications of singular perturbations.* Springer (2000).

Waggoner, J.R., Castillo, J.L., and Lake, L.W. *Simulation of EOR processes in stochastically generated permeable media*, SPE Formation Evaluation (1992) v. 7, no. 2, p. 173-180.

Yang Ch. and Gu Y., *Accelerated mass transfer of CO_2 in reservoir brine due to density-driven natural convection at high pressures and elevated temperatures*, Ind. Eng. Chem. Res., 45 (2006) 2430-2436.

Zimmerman, W.B. and Homsy, G.M. *Viscous fingering in miscible displacements: Unification of effects of viscosity contrast, anisotropic dispersion, and velocity dependence of dispersion on nonlinear finger propagation*. Physics of Fluids A, 4 (1992) 2348–2359.

Appendix A: Matched Asymptotic Expansions

We consider the equation

$$\varepsilon \frac{d^2}{dx^2} c(x) + \frac{d}{dx} c(x) = a \tag{A.1}$$

where ε is a small Peclet number and x a dimensionless space coordinate, and a source term. The boundary conditions read $c(x = 0) = 0$ and $c(x = 1) = 1$.

The exact solution is given by

$$c(x) = \left(1 - a\right) \frac{e^{-\frac{x}{\varepsilon}} - 1}{e^{\frac{-1}{\varepsilon}} - 1} + ax \tag{A.2}$$

The solution away from the boundary can be approximated as the solution obtained with $\varepsilon = 0$, i.e., $dc_o / dx = a$, which only needs to satisfy only the outer boundary condition $c_o(x = 1) = 1$. The solution is

$$c_o(x) = a(x - 1) + 1. \tag{A.3}$$

Using a coordinate transformation $X = x / \varepsilon$ we can write Eq. (A.1) as

$$\frac{d^2}{dX^2} c_i(X) + \frac{d}{dX} c_i(X) = a\varepsilon. \tag{A.4}$$

The boundary conditions read $c_i(X = 0) = 0$ and $c_i(X = 1 / \varepsilon) = 1$. The outer boundary condition is only stated for easy reference. Without the outer boundary condition the solution in the limit that $\varepsilon = 0$ is any multiple of $\left(1 - \exp(-X)\right)$, i.e., $\beta\left(1 - \exp(-X)\right)$, where β is an arbitrary constant. Imposing the outer boundary condition would give in the limit that $\varepsilon \to 0$ a multiplicative factor of unity, but the exact solution shows that this is incorrect. The outer boundary condition must be dropped for the inner solution in the same way that the inner boundary was dropped for the inner solution. Instead the inner solution must be matched to the outer solution using the matching principle, i.e.,

The *m* term inner expansion of the *n* term outer expansion =

The *n* term outer expansion of the *m* term inner expansion (A.5)

The *m* and *n* can be taken as any two integers. By definition the *m* term inner expansion of the *n* term outer expansion is found by rewriting it in inner variables, expanding asymptotically for small ε and truncating the results to *n* terms. The inner solution $\left(1 - \exp(-X)\right)$ rewritten in outer variables reads $\beta\left(1 - \exp(-x / \varepsilon)\right)$. This solution truncated at zeroth (or any higher order for that matter) in ε reads $c_i^\varepsilon = \beta$. The outer solution written in terms of inner variables reads $c_o^\varepsilon = a\left(\varepsilon X - 1\right) + 1$. Until zeroth order we find $\beta = 1 - a$.

$$c_o(x) = a\left(x - 1\right) + 1 \qquad \text{for the outer solution} \qquad \text{(A.6)}$$

$$c_i(X) = \left(1 - a\right)\left(1 - \exp(-X)\right) \qquad \text{for the inner solution} \qquad \text{(A.7)}$$

The comparison between the inner and outer solutions to the exact equation is given in Figure A.1.

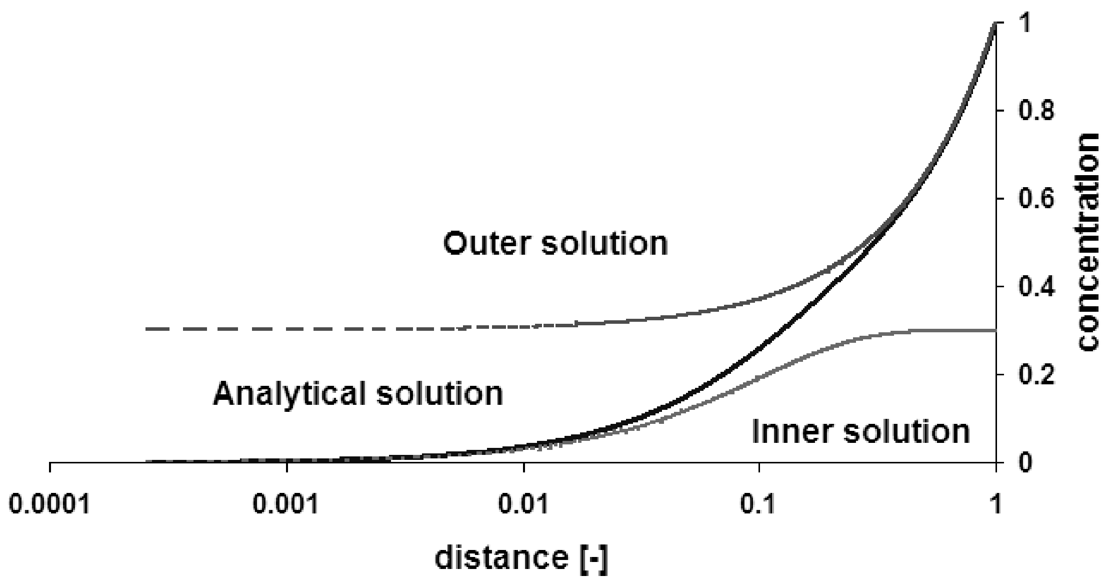

Figure A.1: Inner solution (Eq. 7) and outer solution (A.6) and exact solution of Eq. (A.2)